Journal of Materials Chemistry A

PAPER

View Article Online
View Journal | View Issue

Cite this: J. Mater. Chem. A, 2015, 3, 13445

Preparation of a graphene-based composite aerogel and the effects of carbon nanotubes on preserving the porous structure of the aerogel and improving its capacitor performance†

Zhihua Ma,[ab] Xiaowei Zhao,[ab] Chunhong Gong,[cd] Jingwei Zhang,*[abc] Jiwei Zhang,[ab] Xiufang Gu,[ab] Lei Tong,[ab] Jingfang Zhou[c] and Zhijun Zhang*[ab]

Received 12th March 2015
Accepted 3rd May 2015

DOI: 10.1039/c5ta01831e

www.rsc.org/MaterialsA

A graphene-based aerogel is a promising candidate to be used as a novel supercapacitor due to its unique three dimensional interconnected porous structure and high specific surface area. However, the rolling press process is generally applied in the fabrication of a supercapacitor, in order to reduce contact resistance and upgrade specific volume capacitance. This process tends to deform or destroy the porous structure, and significantly prevents the obtained supercapacitor from achieving its expected performance. In order to improve the pressure resistance of graphene-based aerogels during the rolling press process, a carbon nanotube supported graphene-based composite aerogel (GCA/CNT) with a high specific surface area of 811.5 m^2 g^{-1} was fabricated using a facile two-step process. It was found that the incorporation of carbon nanotubes into the graphene-based aerogel can effectively enhance its pressure resistance and significantly reduce the deformation of the porous structure, especially in the mesoporous region. Furthermore, the resulting GCA/CNT composite aerogel exhibited a remarkably improved electrical conductivity and subsequent superior rate performance due to the formation of a graphene/carbon nanotube three dimensional conductive network.

1. Introduction

There is an urgent demand for the development of inexpensive and environmentally friendly energy storage devices to meet the increasing requirements of consumer electronics, industrial power and other applications.[1–4] Supercapacitors,[5–8] also known as electrochemical capacitors or ultracapacitors, are remarkably attractive energy storage devices due to their high power capacitance, long cycle life and wide thermal operating range,[9,10] making them potential substitutes for conventional storage devices.

Graphene is an outstanding candidate for supercapacitor electrodes with a unique two dimensional (2D) structure.[11,12] Single-layer graphene, composed of sp^2-bonded carbon, can potentially combine the advantages of high specific surface area (SSA) and high conductivity. Many methods have been developed to synthesize graphene, in which "chemical exfoliation of graphite" holds the greatest probability for large scale production[13] due to its low cost and the requirement for equipment is less. However, the as-prepared graphene sheets have a strong tendency to restack in the processes of reduction[14] and subsequent drying process[15] due to the strong π–π interaction among single-layered graphene sheets and their high respect ratio, leading to a serious decrease of SSA and a subsequent poor electrochemical performance. For example, Nguyen *et al.*[14] used hydrazine hydrate to reduce the oxygen groups on the graphene sheets and the obtained sample demonstrated a high degree of agglomeration of the graphene oxide sheets upon reduction. To overcome the undesirable restacking of graphene sheets and prepare high SSA graphene-based materials, many techniques have been developed, including thermal expansion,[16–19] soft or hard template method[20–23] and combination with spacer materials.[24–28]

Recently, three dimensional (3D) graphene aerogels have drawn more and more attention due to their unique assembly process, resulting in significant reduction of undesirable restacking and overlaps. Meanwhile, graphene aerogels demonstrate lots of other advantages, such as high SSA, excellent electrical conductivity and good mechanical property. Shi *et al.*[29] reported the use of a graphene aerogel prepared by a

[a]Key Laboratory of Ministry of Education for Special Functional Materials, Henan University, Kaifeng, 475004, P. R. China. E-mail: jwzhang@henu.edu.cn; zhangzhijun@henu.edu.cn

[b]Collaborative Innovation Center of Nano Functional Materials and Applications, Henan Province, P. R. China

[c]Ian Wark Research Institute, University of South Australia, Mawson Lakes, SA, 5095, Australia

[d]College of Chemistry and Chemical Engineering, Henan University, Kaifeng, 475004, P. R. China

† Electronic supplementary information (ESI) available. See DOI: 10.1039/c5ta01831e

facile hydrothermal assembly of GO as a supercapacitor material. It exhibited a specific capacity of 175 F g^{-1} in an aqueous electrolyte, which is about 50% higher than those of supercapacitors prepared using reduced GO agglomerate particles. In theory, high SSA results in high specific capacitance. Consequently, different additives, such as polymers[30] and reducing agents,[31] were used to assist the assembling process for the increase of SSA. Worsley *et al.*[30] reported the preparation of a graphene aerogel, employing resorcinol and formaldehyde as the modifiers, and the obtained sample exhibited a specific surface area as high as 584 m^2 g^{-1}. More recently, an edge-to-edge assembled graphene oxide aerogel with a SSA reaching 854 m^2 g^{-1} was prepared by Zhang's group.[32] In a recently published paper, Stein *et al.*[33] prepared a graphene aerogel using the self-assembly of graphene oxide and resol having a SSA of 1019 m^2 g^{-1}. However, the specific capacitance was only 99 F g^{-1} at a current density of 100 mA g^{-1}. Compared with the largely increased SSA, increase of the specific capacitance of the aerogel was much less. The destruction of the 3D structure during high pressure treatment and poor electrical conductivity might impede the improvement of specific capacitance. As graphene-based aerogels normally have low mass density and hold a large volume, the high pressure treatment is necessary for preparing the supercapacitor electrode in order to reduce the contact resistance and increase the specific volume capacitance, which are crucial factors for practical application.[34] During the high pressure treatment, the 3D structure of graphene aerogels with lots of interconnected pores can be seriously destroyed and transformed to a compact paper-like structure resulting in the decrease of both SSA and interconnected pore volume, which are confirmed by the SEM images and nitrogen adsorption–desorption test shown in this paper. Furthermore, many of the additives, used as separators or crosslinking agents to induce the graphene assembling process, such as polymers, have low electrical conductivity, resulting in a dramatic decrease of the conductivity of graphene-based aerogels.

In this work, a carbon nanotube supported 3D graphene-based composite aerogel (GCA/CNT) was prepared by a facile two-step method. In the first step a graphene/resol 3D aerogel (GPA) with a high SSA was prepared, using resol as the modifier, which is essential for the fabrication of a supercapacitor. Carbon nanotubes were then deposited onto the surface of the pores in GPA, using an *in situ* CVD method, in order to alleviate structure destruction during pressure treatment and impede further stacking of graphene layers. Moreover, the added carbon nanotubes may increase the electrical conductivity and improve the electrochemical performance by forming a unique three dimensional electrical conductive network. In addition to carbon nanotubes, the added carbon source at high temperatures may heal the defects of the pyrolyzed resol carbon and graphene sheets,[35,36] which further enhance the electrochemical performance of GCA/CNT.

2. Experimental section

All chemicals were analytical grade and used without any further purification. The strategy of the synthesis of GCA/CNT, as shown in Scheme 1, mainly contains two steps: hydrothermal process and CVD process. In the hydrothermal process, the resol molecules coated on the surface of graphene oxide sheets and then the composite carbon sheets underwent a condensation reaction, leading to the formation of a 3D porous GPA aerogel.[33] In the following CVD process, carbon was deposited onto the surface of aerogel walls, forming a unique 3D porous structure of GCA/CNT.

2.1 Synthesis of GPA

GPA was prepared using a process described in the literature.[33] In a typical process, graphite oxide used in this work was prepared from natural flake graphite according to Hummers' method. A GO (1 mg mL^{-1}) aqueous colloid was prepared by the dispersion of GO in DI water. Then, a high power ultrasonic treatment was carried out to exfoliate the GO sheets. The pH value of the GO aqueous colloid was adjusted to 3 using 0.1 M HCl. Consequently, a stable GO dispersion was formed, which can be stable for weeks without any precipitation. Resol–resin (RF) solution was prepared according to a literature procedure[37] and a solution containing 50 wt% of resol was obtained. Then resol was added into the GO colloid dispersion (60 mL) in a 4 : 1 mass ratio under stirring. After that, the mixture was transported to a Teflon-lined autoclave, followed by a hydrothermal treatment at 180 °C for 24 h. GPA was obtained after freeze–drying of the resulting hydrogel.

2.2 Preparation of GCA/CNT aerogel

In a typical process, GPA was immersed in $Co(NO_3)_2 \cdot 6H_2O$ solution (8 mg mL^{-1}) for 24 h and then dried in a vacuum oven at 60 °C. The sample was subsequently placed in a horizontal quartz tubular reactor, heated to 450 °C at 5 °C min^{-1} and kept for 4 h at 450 °C in a H_2/Ar (H_2, 5 wt%) atmosphere. After that, the temperature was raised to 550 °C and then ethanol (0.6 mL min^{-1}) was added as a carbon source for 45 min in an Ar atmosphere. Finally the system was cooled down to room temperature in an Ar atmosphere. After washing with HCl and water, the CNT supported graphene-based composite aerogel was obtained and is denoted as GCA/CNTs. For comparison, GPA was reduced in an H_2/Ar (H_2, 5 wt%) atmosphere at 450 °C for 4 h and further in an Ar atmosphere at 550 °C for 45 min. The obtained sample is denoted as GCA. To study the carbon-repair effect, GCA/C was prepared using the same process as that of GCA, apart from the addition of ethanol at 550 °C.

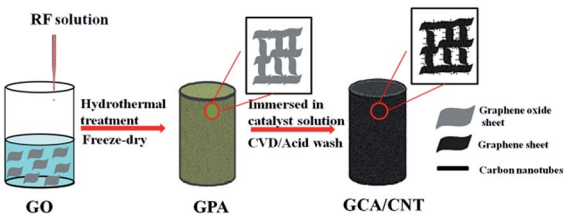

Scheme 1 Synthesis process of GCA/CNT.

2.3 Characterization

The morphology and structure of the aerogels were characterized using scanning electron microscopy (SEM, NOVA NANO-SEM 450) and transmission electron microscopy (TEM, JEM-2010). X-ray diffraction (XRD, Bruker D8 Advance) was performed with Cu K_α radiation ($\lambda = 0.15418$ nm). The Raman spectrum was recorded on a confocal microscopic Raman spectrometer (RM-1000). Nitrogen adsorption and desorption isotherms were measured using an automated surface area and pore size analyzer (SIMP-21) and the specific surface areas of the samples were calculated by the Brunauer–Emmett–Teller (BET) method using the adsorption data.

2.4 Electrochemical measurements

The two-electrode configuration was used to evaluate the electro-capacitive performance. Stainless steel sheets with a diameter of 1.7 cm and Ni foam with a diameter of 1.6 cm were used as current collectors. The active material was mixed with a 5 wt% polytetrafluoroethylene (PTFE) binder and then pressed onto a piece of nickel foam dish under 10 MPa. After that, the dish was dried in a vacuum oven at 120 °C overnight. The mass loading of the active material for each dish was about 12 mg. Electrochemical impedance spectroscopy (EIS) measurements were carried out from 0.1 Hz to 100 kHz at the open circuit potential. The cyclic voltammogram (CV) curves and galvanostatic charge–discharge performance (GDC) were tested on an Arbin test system employing KOH (6.0 mol L^{-1}) solution as the electrolyte. Gravimetric capacitances were calculated according to galvanostatic charge–discharge curves using the following formula:[38]

$$C = \frac{4I}{m\mathrm{d}V/\mathrm{d}t}$$

In the formula, I (A) is the charge–discharge current density (A), m (g) refers to the total mass of both anode and cathode materials, and $\mathrm{d}V/\mathrm{d}t$ can be calculated from the slope of the fitting straight line of the discharge curve.

3. Results and discussion

3.1 Morphology and microstructure of aerogels

The microstructures of GCA and GCA/CNT were observed using the SEM and TEM images. The as-prepared GCA exhibits a well-defined and interconnected 3D network microstructure with uniformly dispersed hierarchical pores with a diameter ranging from nanometers to micrometers, as shown in Fig. 1a. No carbon balls are seen, which is consistent with the result observed before.[33] As shown in Fig. 1c, the aerogel walls, which are made up of graphene sheets and pyrolyzed carbon, are very thin and curved along the surfaces of the assembled graphene sheets. Fig. 1e shows a typical TEM image of GCA, which further confirms the wrinkles and curves along the surface. The SEM images of GCA/CNT are shown in Fig. 1b and d, in which a unique 3D interconnected porous graphene/carbon/carbon nanotubes structure is observed. The enlarged image of GCA/CNT (Fig. 1d) shows that the carbon nanotubes are highly

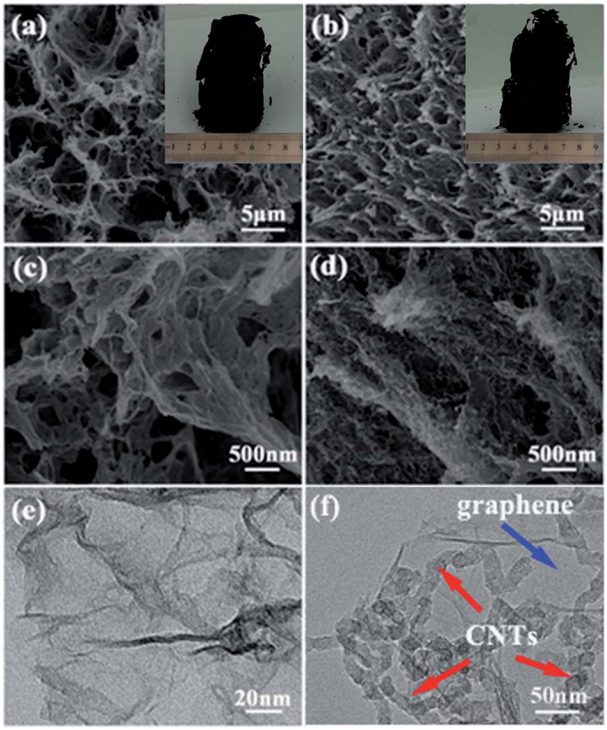

Fig. 1 SEM images of GCA (a and c) and GCA/CNT (b and d); TEM images of GCA (e) and GCA/CNT (f).

curved and uniformly anchor on the surface of the pores with a length of 100–200 nm. The inner and outer diameters of CNTs are about 9 and 18 nm (shown in Fig. S1c†), respectively. In the hydrothermal process, a 3D aerogel of GPA with abundant opening and interconnected pores is obtained, which facilitates the sufficient contact between the catalyst precursor solution and the inner surface of the aerogel, resulting in a uniform distribution of the catalyst particles in the aerogel. Besides, the open and interconnected porous structure provides adequate paths for the carbon source gas to reach the deep inner part of the aerogel. As a result, the full contact of the catalyst and carbon source gas is realized, resulting in the uniform deposition of carbon nanotubes in the following CVD process. No cobalt particles are observed, suggesting the complete removal of the catalyst after acid wash.

XRD patterns of GO, GPA and GCA/CNT are shown in Fig. 2a. A sharp diffraction peak is observed for GO around 10.5°, corresponding to the (002) reflections with a d-spacing value of 0.84 nm, which is attributed to the insertion of the oxide functional groups. For GPA, the peak around 10.5° disappears in the XRD pattern and no obvious peak is observed from 10° to 26°, indicating the presence of well aligned graphene sheets with little overlaps. For GCA/CNT, a broad peak around 26.6° is observed, corresponding to the (002) reflections with a d-spacing value of 0.34 nm. The emergence of a broad peak at 26.6° is attributed to the deposition of carbon nanotubes[39] on the surface, along with the increased graphitic degree of the resol pyrolyzed carbon around the catalyst particles during the CVD process.

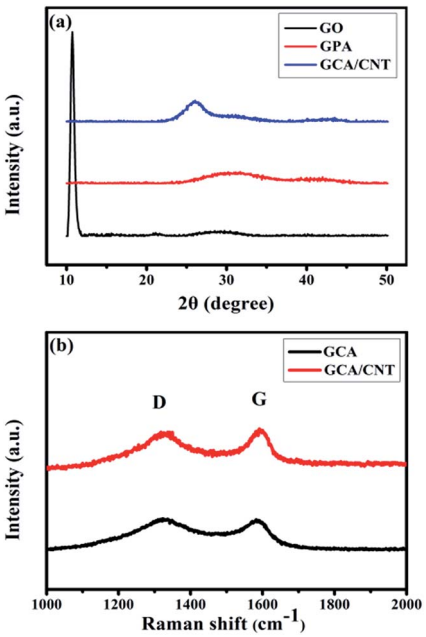

Fig. 2 XRD patterns of GO, GPA and GCA/CNT (a); Raman spectra of GCA and GCA/CNT (b).

The Raman spectra of GCA and GCA/CNT are shown in Fig. 2b. Two primary peaks around 1590 cm^{-1} (G band) and 1325 cm^{-1} (D band) are observed for both of them, indicating the presence of the E_{2g} phonon of sp^2-bonded carbon atoms and the defects in the graphene layers respectively. As is well known, the intensity ratios of the D to G bands reflect the disorder degree of the carbonaceous materials. Comparing the I_D/I_G values between GCA and GCA/CNT, a decrease from 1.02 to 0.90 is obtained, indicating a remarkably improved content of the sp^2 hybridized carbon. The much lower I_D/I_G value of GCA/CNT indicates that the combined carbon nanotubes possess a sp^2 hybridized dominated carbon structure with few defects.

3.2 Morphology and structure changes under high pressure treatment

As the obtained graphene-based aerogels are superlight with low mass density and large volume, the high pressure treatment is necessary for preparing supercapacitor electrodes in order to reduce contact resistance and upgrade specific volume capacitance, which are crucial for practical application. To study the change of the structure during high pressure treatment, GCA and GCA/CNT (12 mg) were pressed onto a piece of Ni foam under 10 MPa and then scraped off for further study, respectively. The obtained samples of GCA and GCA/CNT are denoted as pGCA and pGCA/CNTs, respectively. As shown in Fig. 3a, a compact paper-like structure is observed for pGCA, exhibiting a reduced volume, which is beneficial to the high specific volume capacitance. During the pressure treatment, the 3D porous structure of GCA is seriously destroyed and deformed to a newly formed compact paper-like structure, composed of a number of layers of graphene for each piece. Moreover, the open and interconnected porous structure of GCA is also destroyed

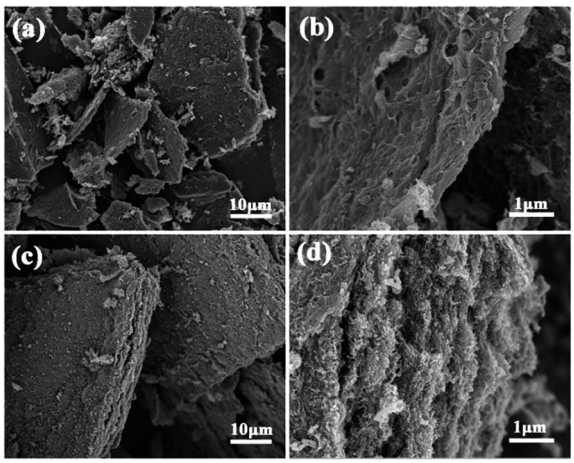

Fig. 3 SEM images of pGCA (a and b) and pGCA/CNT (c and d).

during the pressure treatment and only the pores on the outside surface exist, as shown in Fig. 3b. For pGCA/CNT, the 3D porous structure is also pressed into thick pieces, as shown in Fig. 3c; however, the stacked graphene sheets are much looser (Fig. 3d), with an enlarged layer distance between graphene sheets. The loose state of pGCA/CNT indicates that the uniformly incorporated CNTs alleviate the structure destruction of pGCA/CNT and impede further stacking of graphene layers, leading to an enlarged layer space. Consequently, a unique Hellenic-type structure is obtained with the carbon nanotube support between the graphene layers.

The nitrogen adsorption–desorption isotherms and pore size distribution (inset) of GCA, pGCA, GCA/CNT and pGCA/CNT are shown in Fig. 4. The isotherms show type IV curves for all the four samples. The H3 type hysteresis loop at medium and high pressure ranges indicates slit-like pores distributed in the samples. The BET specific surface area of GCA is calculated to be 891.2 $m^2 g^{-1}$, laying a good foundation for the preparation of the high SSA GCA/CNT aerogel. For pGCA, the curve decreases clearly at high pressure ranges (Fig. 4a), indicating the destruction of the porous structure. The SSA value for pGCA is calculated to be 794.7 $m^2 g^{-1}$, which is decreased by 10.8% compared with the one for GCA. The decrease of SSA is due to the destruction of the 3D porous structure and the stacking of the graphene sheets induced by high pressure treatment, which is confirmed by the SEM images shown in Fig. 3. When it comes to pGCA/CNT, the decrease of the curve in the high pressure range (Fig. 4a) is much less, indicating a better retention of the pore structure. The SSA of GCA/CNT is calculated to be 811.5 $m^2 g^{-1}$, slightly lower than that of GCA, which might be attributed to the incorporation of the low SSA material CNTs. After the pressure treatment, the SSA value for pGCA/CNT is reduced to 780.2 $m^2 g^{-1}$. It is quite remarkable that the reduction percentage is only 3.9%, much less than that from GCA to pGCA. This indicates that the combined CNTs significantly impede further stacking of graphene layers and result in a higher SSA retention during the pressure treatment.

The pore size distribution is a very important factor to explain the structural changes during the pressure treatment.

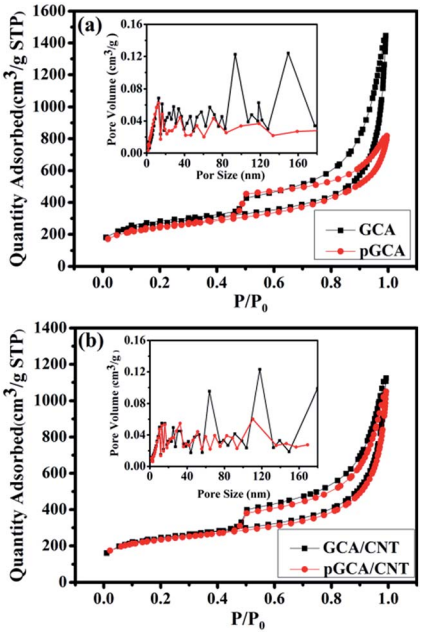

Fig. 4 N_2 adsorption–desorption isotherm and pore size distribution (inset) of GCA and pGCA (a); N_2 adsorption–desorption isotherm and pore size distribution (inset) of GCA/CNTs and pGCA/CNTs (b).

As shown in Fig. 4a (inset), an obviously reduced value in the range of medium (20–60 nm) to large (60–180 nm) diameters for pGCA is observed, compared with the curve of GCA, indicating the destruction of the open and connected mesopores and macropores. As is known, the macropores and mesopores not only provide hierarchical paths for ion diffusion but also shorten the ion diffusion length, resulting in the improvement of the electrochemical performance.[40] In contrast, the destruction of the open and interconnected pores can significantly impede the diffusion of ions and prevent the electrolyte from coming into contact with the inside surface, resulting in the reduction of the electrolyte-accessible surface area. The change of pore size distribution from GCA/CNT to pGCA/CNT was also analyzed and is shown in Fig. 4b (inset). A negligible decrease in the volume of the pores with a diameter of 20–60 nm is observed, suggesting that the destruction of the porous structure is effectively alleviated. During the pressure treatment, the uniformly distributed carbon nanotubes in GCA/CNT act as separation materials and support between graphene layers, preventing the layers from further stacking. As a result, the open and interconnected pores remain, which is favourable for their electrochemical performance.

From the above observations, we propose the transformation mechanisms of pGCA and pGCA/CNT, as shown in Fig. 5, to explain the change of the structure. When GCA is pressed under 10 MPa, the 3D structure with a lot of connected pores is significantly destroyed and the graphene walls of GCA are pressed together forming a compact paper-like structure with only pores on the outermost surface. When GCA/CNT is pressed, the uniformly combined CNTs play the role of separation and supporting materials preventing graphene layers from further stacking. As a result, an incompact CNTs

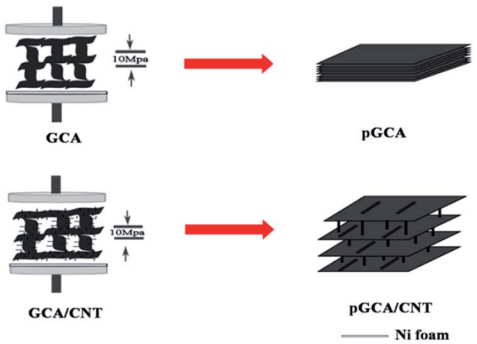

Fig. 5 A schematic diagram of the transformation mechanisms from GCA and GCA/CNT to pGCA and pGCA/CNT.

supported layer structure is obtained with an enlarged layer distance and a number of open and interconnected mesopores are preserved. There are two advantages when GCA/CNT is used as a supercapacitor material: (i) it alleviates the structure destruction during pressure treatment and impedes further stacking of graphene layers, resulting in the formation of an incompact layer structure with an enlarged layer space. As a result the decrease of SSA during pressure treatment is minimized and a large portion of the open and interconnected mesopores survives, facilitating fast diffusion of ions and molecules. Moreover, the reserved pores provide an opportunity for the electrolyte to come into contact with the inside surface, increasing the electrolyte-accessible surface area; (ii) it significantly improves the electrical conductivity.[41] After the pressure treatment, the carbon nanotubes significantly improve the total electrical conductivity due to the formation of a 3D electrical conductive network. As a result, excellent electrochemical performance of GCA/CNT can be achieved.

3.3 Electrochemical performance

It is reported that a carbon rich atmosphere might repair the defects of carbon based materials and improve their electrical conductivity.[35,36] The active sample GCA/C was prepared and the electrochemical performances of GCA, GCA/C and GCA/CNT were characterized by CV test to understand the electrochemical behaviour changes of GCA/CNT. It is observed that all the three electrodes exhibit quasi-rectangular curves at low scan rates of 5 mV s^{-1} (Fig. 6a), showing an ideal double layer capacitive behaviour. Comparing the CV curves at a high scan rate (Fig. 6b), the curves of GCA and GCA/C are dramatically distorted. Notably, the curve of GCA/C is slightly less distorted due to carbon repair with pyrolyzed ethanol. However, the improvement is not significant, which may be attributed to the low temperature resulting in a low graphitic degree of the deposited carbon without the catalyst. On the other hand, the curves of GCA/CNT show a better quasi-rectangular shape suggesting an improved electrical conductivity due to the formation of the 3D electrical conductive network. Meanwhile, the rescued interconnected mesopores provide diffusion paths, shortening the diffusion length and facilitating fast diffusion. The specific capacitance of GCA/CNT is significantly improved

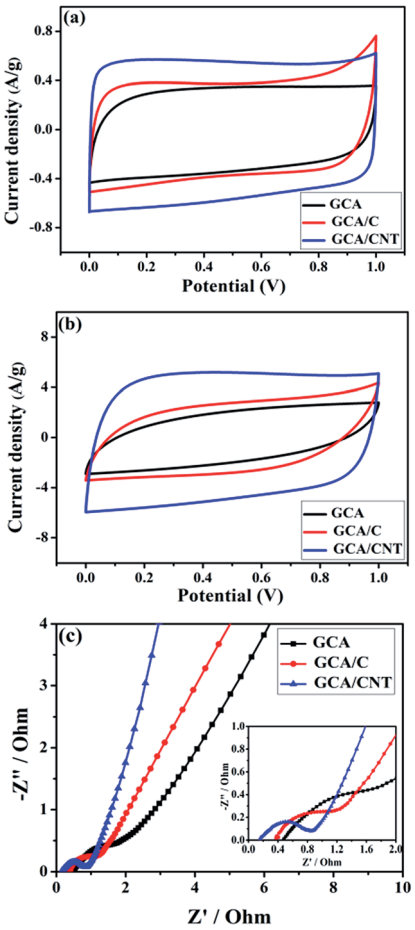

Fig. 6 Cyclic voltammetry curves measured at scan rates of 5 mV s^{-1} (a) and 50 mV s^{-1} (b) for GCA, GCA/C and GCA/CNT; Nyquist plots for GCA, GCA/C and GCA/CNT (c).

with an enlarged area of the CV curve. The combination of CNTs with GCA effectively impedes the stacking of graphene layers during pressure treatment and dramatically enlarges the space between the graphene layers, leading to a higher exposed surface area. Furthermore, the remaining interconnected pores in pGCA/CNT facilitate the diffusion of electrolyte ions deep inside the active material achieving a higher electrolyte-accessible surface area.

In order to fully understand the supercapacitor behaviour, impedance of the samples was measured in the frequency range of 100 kHz–0.1 Hz at an open circuit potential with an AC perturbation of 5 mV (Fig. 6c). The straight line at the low frequency is the result of Warburg resistance showing the rate of ion diffusion/transport in the electrolyte to the electrode surface. The curve of GCA/CNT in the low frequency region is more parallel to the imaginary part, indicating lower diffusion resistance of ions in the active material. The intersection of the curves at the *X*-axis represents the internal resistances or ESR of the electrodes, which are found to be 0.48, 0.41 and 0.15 Ω for GCA, GCA/C and GCA/CNT, respectively. Furthermore, the semicircle diameter of GCA/C is smaller than GCA, indicating an increased electrical conductivity by the carbon repair process. GCA/CNT possesses the smallest semicircle diameter, suggesting a significant improvement of the electrical conductivity, which is attributed to the incorporation of the highly conductive CNT material, resulting in the formation of a 3D conductive network.

The galvanostatic charge–discharge curves of GCA, GCA/C and GCA/CNT at 0.5 and 5 A g^{-1} are shown in Fig. 7. It is noticed that each charge–discharge curve exhibits a good linear shape and a typical triangle symmetrical distribution (Fig. 7a), indicating the typical double layer capacitive behaviour. A dramatic voltage drop, corresponding to I_R, is observed for GCA and GCA/C at 0.5 A g^{-1}. When the current density reaches 5 A g^{-1} (Fig. 7b), rapid voltage drops are found for all the three samples, but the voltage drop of GCA/CNT is the least, which further confirms the improvement of electrical conductivity. A significant improvement of specific capacitance from GCA (116.6 F g^{-1}) to GCA/CNT (212.7 F g^{-1}) is achieved at a current density of 0.5 A g^{-1}. Although GCA possesses the largest SSA, the poor electrical conductivity and serious destruction of its 3D porous structure prevents it from exhibiting its full electrochemical

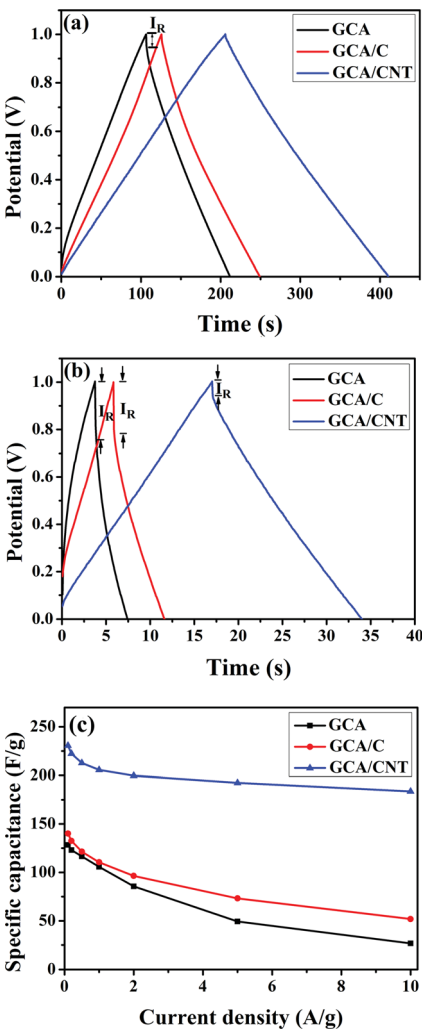

Fig. 7 Galvanostatic charge–discharge curves of GCA, GCA/C and GCA/CNT measured at current densities of 0.5 A g^{-1} (a) and 5 A g^{-1} (b); relationship of the specific capacitance with respect to the discharge specific currents for GCA, GCA/C and GCA/CNT (c).

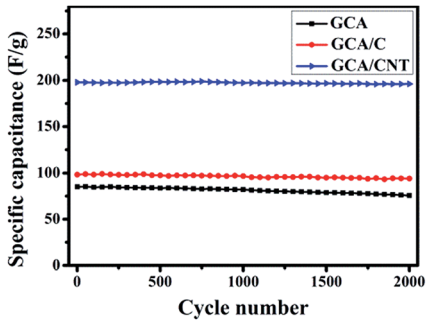

Fig. 8 Average specific capacitance *versus* cycle number for GCA, GCA/C, and GCA/CNT at a current density of 2 A g^{-1}.

performance. For electrical double layer capacitors, the electrochemical performances of materials are greatly dependent on three factors: electrolyte-accessible surface area, electrical conductivity and proper porous structure. For GCA/CNT, the unique carbon nanotubes supported structure significantly alleviates the destruction of the porous structure and improves the electrical conductivity by forming a 3D conductive network, resulting in a significantly improved electrochemical performance.

The rate performances of GCA, GCA/C and GCA/CNT (Fig. 7c) are further summarized by varying the current density in the GDC test from 0.1 to 10 A g^{-1}. It is observed that the specific capacitance of GCA/CNT is much higher than those of GCA and GCA/C at the same current density and the maximum capacitance of 230.6 F g^{-1} is obtained at a current density of 0.1 A g^{-1} for GCA/CNT. Moreover, the capacitance retentions from 0.1 to 10 A g^{-1} are calculated to be 20.8%, 36.9% and 79.6% for GCA, GCA/C and GCA/CNT, respectively. The dramatically enhanced capacitance retention of GCA/CNT is attributed to the incorporation of carbon nanotubes which not only significantly improves the electrical conductivity, but also prevents the graphene layers from further restacking and retains a large number of interconnected pores, providing more effective specific surface area and shortening diffusion lengths.

The electrochemical stabilities of different samples are further investigated by a continuous cycle test at a current density of 2 A g^{-1}. As shown in Fig. 8, a negligible capacitance loss for GCA/CNT is obtained after 2000 cycles, indicating a favourable electrochemical stability and it should be attributed to the good structural stability, which endows GCA/CNT with great potential applications.

4. Conclusions

In summary, a carbon nanotube supported graphene-based composite aerogel with a high specific surface area (811.5 m^2 g^{-1}) was prepared by a facile method. The presence of carbon nanotubes in the aerogel significantly alleviates the destruction of the 3D interconnected porous structure and facilitates the formation of a 3D conductive network during high pressure treatment for the preparation of supercapacitor electrodes, resulting in a remarkably improved electrochemical performance. The supercapacitor prepared using GCA/CNT exhibits a specific capacitance of 230.6 F g^{-1} at 0.1 A g^{-1} in 6 M KOH solution. The present work provides us a new method to fabricate graphene layered materials with controlled layer distance simply by adjusting the size of the intercalated material. The resulting unique 3D porous material can be expected to find many other applications in the fields of, for example, Li ion batteries and hydrogen storage.

Acknowledgements

The financial support from the National Natural Science Foundation of China (Grants 20971037 and 21271063 and 21441004), Innovation Scientists and Technicians Troop Construction Projects of Henan Province (134100510005), Program for Changjiang Scholars and Innovative Research Team in University (no. PCS IRT1126) and Australian Research Council (ARC) Discovery Project (DE120101788) has been greatly acknowledged.

Notes and references

1 J. A. Rogers, T. Someya and Y. G. Huang, *Science*, 2010, **327**, 1603–1607.
2 J. M. Tarascon and M. Armand, *Nature*, 2001, **414**, 359–367.
3 L. Nyholm, G. Nyström, A. Mihranyan and M. Strømme, *Adv. Mater.*, 2011, **23**, 3751–3769.
4 X. Feng, B. D. Yang, Y. M. Liu, Y. Wang, C. Dagdeviren, Z. J. Liu, A. Carlson, J. Y. Li, Y. G. Huang and J. A. Rogers, *ACS Nano*, 2011, **5**, 3326–3332.
5 J. Yan, E. Khoo, A. Sumboja and P. S. Lee, *ACS Nano*, 2010, **4**, 4247–4255.
6 M. K. Liu, W. W. Tjiu, J. S. Pan, C. Zhang, W. Gao and T. X. Liu, *Nanoscale*, 2014, **6**, 4233.
7 Y. Yang, L. Li, G. D. Ruan, H. L. Fei, C. S. Xiang, X. J. Fan and J. M. Tour, *ACS Nano*, 2014, **8**, 9622–9628.
8 J. Lin, C. G. Zhang, Z. Yan, Y. Zhu, Z. W. Peng, R. H. Hauge, D. Natelson and J. M. Tour, *Nano Lett.*, 2013, **13**, 72–78.
9 G. P. Wang, L. Zhang and J. J. Zhang, *Chem. Soc. Rev.*, 2012, **41**, 797–828.
10 Y. Zhu, S. Murali, M. D. Stoller, K. J. Ganesh, W. Cai, P. J. Ferreira, A. Pirkle, R. M. Wallace, K. A. Cychosz, M. Thommes, D. Su, E. A. Stach and R. S. Ruoff, *Science*, 2011, **332**, 1537–1541.
11 F. Liu, S. Y. Song, D. F. Xue and H. J. Zhang, *Adv. Mater.*, 2012, **24**, 1089–1094.
12 L. Peng, X. Peng, B. Liu, C. Wu, Y. Xie and G. Yu, *Nano Lett.*, 2013, **13**, 2151–2157.
13 X. B. Fan, W. C. Peng, Y. Li, X. Y. Li, S. L. Wang, G. L. Zhang and F. B. Zhang, *Adv. Mater.*, 2008, **20**, 4490–4493.
14 S. Stankovich, D. A. Dikin, R. D. Piner, K. A. Kohlhaas, A. Kleinhammes, Y. Y. Jia, Y. Wu, S. T. Nguyen and R. S. Ruoff, *Carbon*, 2007, **45**, 1558–1565.
15 Y. Si and E. T. Samulski, *Chem. Mater.*, 2008, **20**, 6792–6797.
16 M. J. McAllister, J. L. Li, D. H. Adamson, H. C. Schniepp, A. A. Abdala, J. Liu, M. Herrera Alonso, D. L. Milius,

R. Car, R. K. Prud'Homme and I. A. Aksay, *Chem. Mater.*, 2007, **19**, 4396–4404.
17 J. F. Shen, Y. Z. Hu, M. Shi, X. Lu, C. Qin, C. Li and M. X. Ye, *Chem. Mater.*, 2009, **21**, 3514–3520.
18 S. R. Wang, M. Tambraparni, J. J. Qiu, J. Tipton and D. Dean, *Macromolecules*, 2009, **42**, 5251–5255.
19 S. Wakeland, R. Martinez, J. K. Grey and C. C. Luhrs, *Carbon*, 2010, **48**, 3463–3470.
20 M. Y. Yan, F. C. Wang, C. H. Han, X. Y. Ma, X. Xu, Q. Y. An, L. Xu, C. J. Niu, Y. L. Zhao, X. C. Tian, P. Hu, H. G. Wu and L. Q. Mai, *J. Am. Chem. Soc.*, 2013, **135**, 18176–18182.
21 Y. Gu, H. Wu, Z. G. Xiong, W. Al Abdulla and X. S. Zhao, *J. Mater. Chem. A*, 2013, **2**, 451–459.
22 H. Wang, L. Y. Shi, T. T. Yan, J. P. Zhang, Q. D. Zhong and D. S. Zhang, *J. Mater. Chem. A*, 2014, **2**, 4739–4750.
23 H. J. Wang, X. X. Sun, Z. H. Liu and Z. B. Lei, *Nanoscale*, 2014, **6**, 6577.
24 H. R. Byon, B. M. Gallant, S. W. Lee and Y. Shao-Horn, *Adv. Funct. Mater.*, 2013, **23**, 1037–1045.
25 K. Zhang, L. L. Zhang, X. S. Zhao and J. S. Wu, *Chem. Mater.*, 2010, **22**, 1392–1401.
26 C. Zhou, Y. W. Zhang, Y. Y. Li and J. P. Liu, *Nano Lett.*, 2013, **13**, 2078–2085.
27 L. L. Peng, X. Peng, B. R. Liu, C. Z. Wu, Y. Xie and G. H. Yu, *Nano Lett.*, 2013, **13**, 2151–2157.
28 M. Q. Zhao, Q. Zhang, J. Q. Huang, G. L. Tian, T. C. Chen, W. Z. Qian and F. Wei, *Carbon*, 2013, **54**, 403–411.
29 Y. X. Xu, K. X. Sheng, C. Li and G. Q. Shi, *ACS Nano*, 2010, **4**, 4324–4330.
30 M. A. Worsley, P. J. Pauzauskie, T. Y. Olson, J. Biener, J. H. Satcher and T. F. Baumann, *J. Am. Chem. Soc.*, 2010, **132**, 14067–14069.
31 X. T. Zhang, Z. Y. Sui, B. Xu, S. F. Yue, Y. J. Luo, W. C. Zhan and B. Liu, *J. Mater. Chem.*, 2011, **21**, 6494.
32 H. Huang, P. W. Chen, X. T. Zhang, Y. Lu and W. C. Zhan, *Small*, 2013, **9**, 1397–1404.
33 Y. Q. Qian, I. M. Ismail and A. Stein, *Carbon*, 2014, **68**, 221–231.
34 X. Yang, C. Cheng, Y. Wang, L. Qiu and D. Li, *Science*, 2013, **341**, 534–537.
35 V. L. Pez, R. S. Sundaram, C. G. Mez-Navarro, D. Olea, M. Burghard, J. G. Mez-Herrero, F. L. Zamora and K. Kern, *Adv. Mater.*, 2009, **21**, 4683–4686.
36 K. C. Cao, Y. Tian, Y. Z. Zhang, X. D. Yang, C. Y. Bai, Y. Luo, X. S. Zhao, L. J. Ma and S. J. Li, *Nanoscale*, 2014, **6**, 13518–13526.
37 Y. Meng, D. Gu, F. Q. Zhang, Y. F. Shi, L. Cheng, D. Feng, Z. X. Wu, Z. X. Chen, Y. Wan, A. Stein and D. Y. Zhao, *Chem. Mater.*, 2006, **18**, 4447–4464.
38 Q. De Yang and S. Hang, *J. Power Sources*, 1998, **74**, 99–107.
39 Z. J. Fan, J. Yan, T. Wei, G. Q. Ning, L. J. Zhi, J. C. Liu, D. X. Cao, G. L. Wang and F. Wei, *ACS Nano*, 2011, **5**, 2787–2794.
40 D. S. Su and R. Schlögl, *ChemSusChem*, 2010, **3**, 136–168.
41 Z. Y. Sui, Q. H. Meng, X. T. Zhang, R. Ma and B. Cao, *J. Mater. Chem.*, 2012, **22**, 8767–8771.